Fragmentation of One-Dimensional Monatomic Chains under Tension: Simulation and Statistical Theory

ARTICLE *in* THE JOURNAL OF PHYSICAL CHEMISTRY · MARCH 1995

Impact Factor: 2.78 · DOI: 10.1021/j100009a005

3 AUTHORS:

Kim Bolton
Högskolan i Borås
140 PUBLICATIONS **2,542** CITATIONS
SEE PROFILE

Sture Nordholm
University of Gothenburg
215 PUBLICATIONS **3,496** CITATIONS
SEE PROFILE

Harold W. Schranz
47 PUBLICATIONS **728** CITATIONS
SEE PROFILE

Fragmentation of One-Dimensional Monatomic Chains under Tension: Simulation and Statistical Theory†

Kim Bolton* and Sture Nordholm

Department of Physical Chemistry, University of Göteborg and Chalmers University of Technology, S-412 96 Göteborg, Sweden

Harold W. Schranz

Research School of Chemistry, Australian National University, Canberra, ACT 0200, Australia

Received: August 2, 1994; In Final Form: November 22, 1994[⊗]

A one-dimensional monatomic chain under tensile stress has been studied by molecular dynamics. The aim is to determine the lifetime to chain breakage and to ascertain whether this event can be described by simple statistical reaction rate theory. Chains of 2−20 atoms have been simulated. A simple transition state theory, equivalent to a nucleation theory for one-dimensional fluids, gives the main features of the decay rate coefficient as a function of the applied stress. For finite chain lengths an anharmonic RRKM theory provides a more accurate rate coefficient, but chain healing (reversible decay) in the simulated motion causes a significant deviation, particularly at high chain energy. The simulation is extended to chain arrays which show greatly increased nonstatistical effects.

Introduction

Despite the great success of the simple transition state theory (TST)[1] and the RRKM theory,[1,2] it is now well understood that chemical reaction rates display nonstatistical effects to varying and yet unknown extent. The true role of the internal dynamics lies somewhere between the internal equilibrium assumptions of TST and RRKM theory and the totally nonergodic theory of Slater[3] where the internal energies of the vibrational modes are constants of the motion. Experiments tend to favor the RRKM theory as opposed to the Slater theory,[4−6] but the evidence for nonstatistical molecular decay is mounting. Slow internal vibrational redistribution (IVR) has been observed in the decomposition of allyl isocyanide[7] and methylbicyclobutyl.[8] Molecular dynamics (MD) simulations of van der Waals clusters[9] and polyatomic molecules such as H_2O_2,[10] Si_2H_6,[11−13] and 1,2-$C_2H_4F_2$[13,14] have reinforced the expectation of IVR which may be incomplete on the time scale of reaction.

The mechanisms underlying the IVR process have therefore been the subject of extensive investigations[15] which have included MD studies of chain systems.[16] A true *a priori* calculation of an experimental reaction rate is, however, rarely possible due, in part, to the numerical difficulties of dealing with quantum dynamics and a lack of potential energy surface information. Classical dynamics can, however, be expected to show patterns of nonstatistical effects that are similar to the corresponding quantum dynamics,[17,18] and simulations performed on simple potential surfaces are expected to yield information of a general nature. One-dimensional chain molecules provide a class of simple but nontrivial systems which have attracted considerable interest in connection with ergodic properties and IVR rates at least since the work of Fermi, Pasta, and Ulam.[19] Due to their simplicity, such systems are ideal for illustrating and understanding the mechanisms controlling the IVR process, the transition from quasi-periodic to chaotic dynamics, and the relationship between classical and quantum dynamics.[20,21] Extensive MD simulations of one-dimensional chain molecule decomposition have been carried out to test the applicability of RRKM analysis to the decay of such molecules.[22−24] The results showed that uniform Morse bonded chains conformed well with RRKM analysis at energies just above the threshold to decay but less well as the internal energy increased. However, anharmonic effects had to be included in the density of states which determines the rate coefficient for decay, and the nonstatistical effects increased rapidly if the chains were made nonuniform by varying the masses and/or bond strengths.

In the present work we revisit the one-dimensional chain simulations, but now we apply a tensile stress (tension) to the chains. As illustrated in Figure 1, this has the effect of producing bond potentials with well-defined potential barriers. Thus, the RRKM analysis incorporates an internal (tight) transition state rather than the loose transition state of the chains in the earlier work.[22−24] We also consider the fission of arrays of chains such as that shown in Figure 2. The presence of neighboring chains is expected to increase or introduce nonstatistical effects such as barrier recrossing. Such systems are of interest when investigating the tensile strength of polymers, *e.g.*, when bridging interacting particles in colloidal dispersion or forming fibers in synthetic materials.

An equivalent description of a chain under tension is that of a chain under negative pressure (where *negative* pressure reflects the fact that it is a *tensile* stress).[33] The rate of chain fission (or, alternatively, the rate of formation of a hole in the strained chain) can then be thought of in terms of homogeneous nucleation theory where the rate of bubble formation in a metastable liquid—which can be obtained by decompressing the liquid—is of importance. Current theories describing the rate of bubble formation and growth are formulated in terms of statistical thermodynamics combined with hydrodynamic considerations[25,26] and subsequently require knowledge of the macroscopic properties of the system. However, it should also be possible to describe the initial stage of nucleation (which is the formation of a "hole" or bubble in the liquid)—and possibly also the later stages of bubble growth—in terms of the microscopic properties of the liquid molecules. Thus, even

† This paper is dedicated to Stuart A. Rice on his 60th birthday.

[⊗] Abstract published in *Advance ACS Abstracts,* February 1, 1995.

0022-3654/95/2099-2477$09.00/0

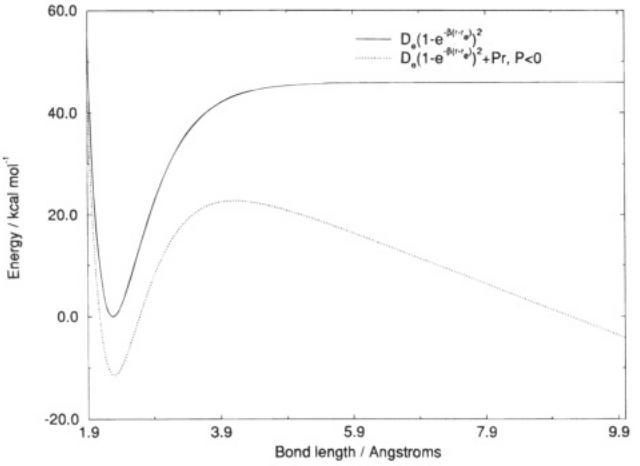

Figure 1. Application of a tensile stress to a Morse potential (solid line) leads to a lowering of the equilibrium energy, a longer equilibrium bond length, a well-defined transition state, and a pressure-dependent barrier height (dotted line).

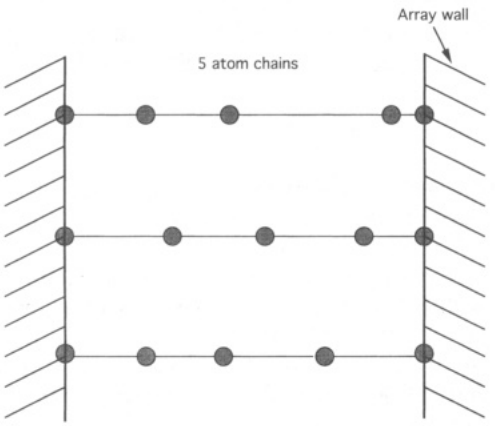

Figure 2. Diagrammatic representation of a three-chain array with five atoms in each chain. The mass of the array walls is equal to the number of chains comprising the array multiplied by the mass of the chain atoms.

though our one-dimensional chain is a severe oversimplification of a three-dimensional liquid where phase transitions occur, we will introduce the isobaric TST as a nucleation theory. We also take a step in the direction of the realistic three-dimensional system by extending the theory to include array dissociation. Nonstatistical effects that may be associated with array dissociation are also expected to appear in systems of higher dimensionality. The theory presented here can therefore be viewed as a first step toward a more complete microscopic nucleation theory.

In the next section we present a detailed description of the nucleation theory in terms of our chain models. We also give a brief summary of the corresponding RRKM theory and present the MD method used to propagate the trajectories together with the Monte Carlo (MC) methods used to generate initial conditions. The third section is devoted to the presentation and discussion of the decay patterns of the strained chains which are compared with statistical predictions. Our conclusions are given in the last section.

Model and Methods

Single-Chain Systems. The five chains that have been investigated consist of 2, 3, 5, 10, and 20 atoms connected by Morse bonds. The Hamiltonian for a single chain is

$$H = \sum_{i=1}^{N-1} \phi(r_i) + \sum_{i=1}^{N} {}^1\!/_2 m_i v_i^2 + Pr_c \tag{1}$$

where N is the number of atoms in the chain, r_i the bond lengths, v_i the atomic velocities, P the pressure, and r_c the chain length. $\phi(r_i)$ has the usual Morse functional form, *i.e.*, $\phi(r_i) = D_e(1 - e^{-\beta(r_i - r_e)})^2$. The Morse parameters $D_e = 45.889$ kcal mol^{-1}, $\beta = 1.94$ Å^{-1}, and $r_e = 2.28$ Å are, to provide a chemical reference, chosen to be the bromine molecule intramolecular interaction parameters that have been used in previous investigations.[22,27] The mass, m_i, is 79.9 amu, which is the atomic mass of bromine.

The one-dimensional chain system of pair potentials acting between neighboring atoms is particularly simple to study by statistical mechanics since in the isobaric ensemble, where the known constants are the particle number, N, the pressure, P, and the temperature, T, the bond lengths become independent variables with a bond length probability density

$$\varrho(r_i) = \frac{e^{-\beta(\phi(r_i)+Pr_i)}}{\int_0^\infty dr_i\, e^{-\beta(\phi(r_i)+Pr_i)}} \tag{2}$$

where $\beta = 1/k_b T$.

If the pressure is negative, then the normalization integral diverges and the system becomes infinitely dilute in equilibrium. However, it is possible to determine a metastable state by assuming that each bond length is less than the value r_m, which is the location of the maximum in the effective potential

$$\phi_{\text{eff}}(r_i) = \phi(r_i) + Pr_i \tag{3}$$

for negative P. The shape of this effective potential is illustrated in Figure 1. Both r_m and the barrier height decrease as the pressure becomes more negative. We can now use the bond length probability density

$$\varrho(r_i) = \frac{e^{-\beta\phi_{\text{eff}}(r_i)}}{\int_0^{r_m} dr_i\, e^{-\beta\phi_{\text{eff}}(r_i)}} \tag{4}$$

to describe the metastable one-dimensional fluid where all bonds are intact, *i.e.*, $r_i < r_m$, $i = 1, \ldots, N-1$. Given that all velocities are thermally distributed, we can apply the classical form of the transition state theory to obtain the rate coefficient for the decay of a single bond,

$$k_{b1}(T) = (2\pi\mu\beta)^{-1/2} \frac{e^{-\beta\phi_{\text{eff}}(r_m)}}{\int_0^{r_m} dr_i\, e^{-\beta\phi_{\text{eff}}(r_i)}} \tag{5}$$

Here μ is the reduced mass of the bond, *i.e.*,

$$\mu = \frac{m_R m_L}{m_R + m_L} \tag{6}$$

where m_R and m_L are the masses of the atoms on the right (R) and left (L) of the bond. In a uniform chain μ is just half of the atomic mass. If the potential is deep and harmonic in the relevant region around the minimum and the pressure is not too high, then we can evaluate eq 5 in a harmonic approximation[34] to get

$$k_{b1}(T) \approx \nu e^{-E_0(P)/k_b T} \tag{7}$$

where ν is the diatomic vibrational frequency (corresponding to a chain of two atoms) and $E_0(P)$ is the pressure-dependent barrier height. In the case of the Morse potential used here we readily find

$$\nu = \frac{\beta}{\pi}\sqrt{\frac{D_e}{\mu}}; \quad E_0(P) = D_e\left(1 + \frac{2P}{\beta D_e}\right)^{1/2} + \frac{P}{\beta}\ln\left[\frac{1 + (1 + 2P/\beta D_e)^{1/2}}{1 - (1 + 2P/\beta D_e)^{1/2}}\right] \quad (8)$$

The probability that the chain will remain intact (no bond broken) at time t is then

$$R_N(t) = e^{-(N-1)k_{b1}t} \quad (9)$$

The decay rate of the chain is then exponential with a rate coefficient

$$k_{bN}(T) = (N-1)k_{b1} \approx (N-1)\nu e^{-E_0(P)/k_bT} \quad (10)$$

Consider now the case of an array of chains (*e.g.*, a polymeric wire). The system is shown in Figure 2. The one-dimensional stress on each unbroken chain is

$$P_{N_{ch}} = P/N_{ch} \quad (11)$$

where N_{ch} is the number of chains in the array. The probability that the array is completely intact at t is then

$$R^{N_{ch}}(t) = e^{-N_{ch}(N-1)k_{b1}t} \quad (12)$$

where k_{b1} is evaluated at $P_{N_{ch}}$.

Once a bond is broken, the stress on the remaining chains rises to $P_{N_{ch}-1}$, and the lifetime to the next bond break decreases correspondingly. The expected lifetime to decay is

$$\tau = \tau_{N_{ch}} + \tau_{N_{ch}-1} + \ldots + \tau_1 \quad (13)$$

where the lifetime of an array with N_i chains intact, τ_{N_i}, is

$$\tau_{N_i} = \frac{\int_0^\infty dt\, te^{-N_i(N-1)k_{b1}(P_{N_i})t}}{\int_0^\infty dt\, e^{-N_i(N-1)k_{b1}(P_{N_i})t}} = [N_i(N-1)k_{b1}(P_{N_i})]^{-1} \quad (14)$$

The dependence of the single bond rate constant on the stress experienced by each of the N_i intact chains is shown explicitly.

Note that these results all depend on the transition state theory being valid; *i.e.*, thermal equilibrium in the "unbroken" configuration space is assumed to hold at all times. In the case of the wire the sequential bond breakage assumed is formally outside the normal single-step transition state theory. It corresponds to a rate coefficient

$$k_{bN}^{N_{ch}}(T) = 1/\tau = 1/\sum_{i=1}^{N_{ch}}[N_i(N-1)k_{b1}(P_{N_i})]^{-1} \quad (15)$$

Errors that arise may stem from the nonergodicity of the chain dynamics and chain healing (recrossings). The nucleation theory presented here allows the dominant role of the pressure to be examined. In this picture the break would occur when the pressure is sufficiently low to cause the rate coefficient to fall in an observable time scale, *i.e.*, approximately 1 s^{-1}. The pressure dominates because it controls the barrier height, which in turn is the dominant factor determining the rate coefficient. An example of the application of this theory to regions where the decay lifetime is accessible by experimentation and where it can be obtained from MD simulation is shown in Figure 3. Thus, the decay of a single chain of 10 atoms at a temperature of 300 K (solid curve) can be predicted over a large pressure range. The accuracy of the theory can be tested by MD techniques in the region where decay lifetimes are sufficiently short (of the order of picoseconds or nanoseconds) to warrant the efficient use of these methods. The MD technique that is described below was used to generate the ranges of lifetimes (shown as the distance between vertically aligned diamonds) in Figure 3. As will be discussed below, the decay ranges—as opposed to single-value decay rates—are a result of the multiexponential shape of the decay curves. The results that will be presented below show that the chain systems behave more statistically at less negative pressures, and hence the predictions made by the theory are also expected to be accurate at the lower pressures required for the longer lifetimes that can be observed experimentally. The dotted curve in the figure shows the (logarithm of the) decay lifetimes of a seven-chain array (10 atoms in each chain) at a temperature of 550 K. The increase in lifetime with the number of chains in the array is expected since the tension is distributed over the chains in the array. Once again it should be noted that higher temperatures and more negative pressures are required to reduce the predicted array lifetime to an extent where it can be checked using MD simulations. If the predictions are accurate at these elevated temperatures and pressures, then they should be accurate at the lower temperatures shown in the figure (based on the trend in the statistical nature of the array systems to be discussed).

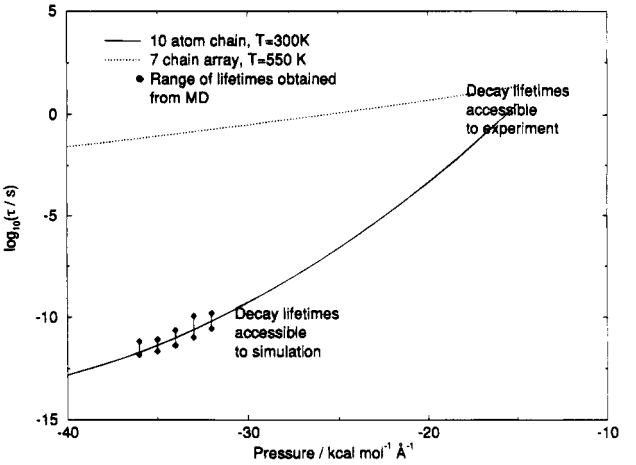

Figure 3. Logarithm of the predicted decay lifetimes of a single chain of 10 atoms (solid curve) and a seven-chain array with 10 atoms in each chain (dotted curve) as a function of pressure. Predictions can be checked using MD simulations in the short lifetime region. The ranges of decay rates obtained from MD (see text) are shown as the displacement between vertically aligned diamonds.

We have associated a range of decay rates with each decay curve determined by MD methods since it is seldom that such a decay curve shows strictly single-exponential behavior. This can be due to nonstatistical features of the decay dynamics (discussed below) or to the fact that a finite length chain is being used in the canonical simulations. Even if the microcanonical decay curves of a particular chain are single exponential, the canonical decay curve can be obtained as a Boltzmann distribution of the single energy decay curves, and the resulting thermal decay curve will therefore not, in general, be single exponential. This problem, which is associated with using chains of finite

TABLE 1: Nucleation Theory Rate Constant, $k(T)$, and the Microcanonical Rate Constant, $k(E)$, as a Function of the Number of Atoms Forming the Chain, N[a]

N	$k(T)/ps^{-1}$	$k(E)/ps^{-1}$
10	0.061	0.003
50	0.330	0.254
100	0.667	0.600
500	3.360	3.311

[a] The data were obtained at a temperature of 3000 K and a pressure of -1 kcal mol^{-1} Å^{-1}.

length in the MD simulations, is reduced as the temperature is decreased or the length of the chain is increased since the effects of fluctuations in the chain energy are minimized in these limits.

In general, it is difficult to separate the two effects (*i.e.*, nonstatistical dynamics and finite chain simulations) that necessitate the introduction of a decay range. We have seen that the influence of using a chain of finite length often overshadows the effect caused by nonstatistical features that may be present in the decay process. In order that we can study the latter, more interesting phenomenon, we will limit ourselves to a discussion of the data obtained from microcanonical MD simulations. We have observed that the nonstatistical effects that appear under these conditions also appear in the corresponding canonical system. Comparison will be made between the microcanonical MD data and RRKM theory which, when anharmonicities are explicitly taken into account, is formally equivalent to our nucleation theory; *i.e.*, the rate of decay determined by the nucleation theory equals the Boltzmann-weighted microcanonical decay rate. In fact, as shown in Table 1, the microcanonical rate, $k(E)$, approaches the nucleation theory rate, $k(T)$, as the chain length increases (and the effects of fluctuations in the chain energy become insignificant). This limiting correspondence between $k(E)$ and $k(T)$, where E is the thermal average energy $\langle E\rangle_T$, has been noted previously in connection with TST.[28] It is analogous to the experimental and theoretical correspondence found by Troe *et al.*[29] in comparisons of UV spectra obtained under conditions of laser and thermal excitation.

Three RRKM decay rate constants were calculated at each energy, pressure, and chain length; the harmonic RRKM decay constant (k_{NM}), the anharmonic RRKM decay constant calculated using the reduced mass of the dissociating chain fragments ($k_{anh,frag}$), and the anharmonic RRKM decay constant based on the reduced mass of the atoms forming the dissociating bond ($k_{anh,atom}$). The motivation for considering these three forms of the RRKM theory is as follows:

1. Harmonic RRKM theory is the simplest form of the theory and is widely used as a method to predict chemical decay rates.

2. The more accurate form of the RRKM theory that is obtained when correctly accounting for anharmonic effects corresponds (in the microcanonical regime) to the nucleation theory discussed above.

3. Since the reaction coordinate is considered to be a local mode, it is appealing to use the masses of the atoms forming the bond when calculating the reduced mass of the reaction coordinate. However, it has been seen[22] that the incorporation of the chain fragment masses sometimes yield rates constants in better agreement with MD decay results. Hence, both $k_{anh,atom}$ and $k_{anh,frag}$ are calculated. Although a brief description of the methods used to determine these rate constants is given here, the reader is referred to a previous paper[22] for details.

The classical form of the RRKM (or RRK) theory was used since comparison is made to classical trajectory calculations. The harmonic RRKM rate constant for a chain with energy E is determined from

$$k_{NM}(E) = \sum_{j=1}^{N-1} k_{j,j+1}(E) \tag{16}$$

where $k_{j,j+1}(E)$ is the decay rate of the $j, j+1$ dissociation channel and is given by

$$k_{j,j+1}(E) = A_j\left[\frac{E - E_0^j}{E}\right]^{s-1} \tag{17}$$

s is the number of dissociation channels, and A_j is given by

$$A_j = \frac{\prod_{i=1}^{s} \nu_i}{\prod_{i=1}^{s-1} \nu_{ji}^{\ddagger}}, \quad j = 1, ..., N-1 \tag{18}$$

ν_i and $\nu_{ij}^{\ddagger}$ are the internal normal mode frequencies of the reactant and transition state, respectively. E_0^j is the well depth along the reaction coordinate which is assumed to be the local mode bond coordinate. The energy, E, is the energy above the zero energy level which is taken to be the bottom of the well and is thus pressure dependent (see Figure 1).

The determination of the rate constant in this manner neglects the anharmonic character of the Morse potential. This can be taken into account by calculating the decay rate of the $j, j+1$ dissociation channel according to

$$k_{j,j+1}(E) = W_N^j(E - E_0^j)/h\varrho_N^I(E) \tag{19}$$

where $\varrho_N^I(E)$ is the internal density of states of the reactant molecule obtained from successive convolutions over the bonds comprising the chain. The sum of states of the jth transition state is

$$W_N^j(E) = \int_0^E d\epsilon\, \varrho_N^j(\epsilon) \tag{20}$$

and, due to the assumption of a separable reaction coordinate, is calculated by convolutions over the bonds of the dissociating fragments. When determining the anharmonic rate constant in this way, the reduced mass associated with the dissociating chain appears in the calculations due to the kinetic coupling between the local modes. In accordance with the assumption that the reaction coordinate is a local mode, this mass should be the reduced mass of the atoms that form the dissociating bond. This yields the rate constant $k_{anh,atom}$. In addition, without claim to theoretical justification, we also consider a reduced mass in terms of the mass of the separating chain fragments. This partially accounts for the atoms surrounding the breaking bond and has been shown to give good agreement between the predicted and MD determined decay rates.[22] It yields the rate coefficient $k_{anh,frag}$.

Microcanonical Monte Carlo sampling procedures were employed for initial MD trajectory configuration selection. The selection procedure has been discussed in detail in a previous paper[22] and is summarized as follows:

1. The procedure is begun with the chain in its minimum potential energy configuration (*i.e.*, all bonds at their equilibrium length), and the statistical weight is calculated as

$$W_i = [E - V_{N,eq}(r,P)]^{(N-3)/2} \tag{21}$$

where $V_{N,eq}(r,P)$ is the potential energy of the chain in this configuration (and is a function of the bond lengths and pressure).

2. A new (trial) configuration is obtained by altering a single bond length, r_i, by a small random perturbation. A maximum value for this perturbation is chosen so that an acceptable rejection ratio of the trial states is obtained.

3. The statistical weight of this trial state is calculated as

$$W_{trial} = 0, \quad V_N \geq E \text{ or } r_i > r_{i,ts}$$
$$= [E - V_N(r,P)]^{(N-3)/2}, \quad V_N < E \text{ and } r_i \leq r_{i,ts} \quad (22)$$

$V_N(r,P)$ is the potential energy of the chain at the trial configuration, and $r_{i,ts}$ is the critical bond length.

4. If $W_{trial} \geq W_i$ the trial state is accepted, while if $W_{trial} < W_i$ a random number, R, where $0 < R < 1$, is compared with W_{trial}/W_i. If $W_{trial}/W_i > R$ the trial state is accepted; otherwise it is rejected.

5. If the trial state was accepted,

$$W_{i+1} = W_{trial} \quad (23)$$

otherwise

$$W_{i+1} = W_i \quad (24)$$

The repetition of these steps forms the Markov chain that is used to select the spatial coordinates. The selection of the momenta is done according to a Gaussian distribution. Muller's method[30] is used to select an initial set of Gaussian distributed numbers ranging from $-\infty$ to ∞. These values are then scaled[22] to give the velocities of the atoms so that the correct kinetic energy, $E - V_N(r,P)$, is obtained. In this way a complete set of microcanonically determined coordinates is obtained.

The decay plots that were used to determine the MD decay rates were obtained from an ensemble of 500 trajectories for all chain lengths, except the diatomic chain where 5000 trajectories were used. The trajectories were propagated using a Gauss–Radau integrator with a fixed time step of 0.5 fs. This gave energy conservation of at least 10 significant figures over a 10 ps trajectory.

Two decay plots were obtained at each energy, pressure, and chain length: The first was calculated based on the assumption that the chain had dissociated when any bond length had exceeded the critical length, r_m. This neglects the effects of recrossings in accordance with the assumption of no recrossing made in the RRKM theory. The second decay plot incorporated the effect of recrossings as follows: The bond lengths of all the bonds were monitored over the entire trajectory, and the time at which any bond length exceeded r_m was recorded. If a bond recrossed back into reactant phase space (*i.e.*, if a bond that had exceeded r_m shortened to a length below r_m), then the next time that it's length exceeded r_m was monitored. This was continued until any bond length had exceeded 10 times the critical bond length, at which stage the chain was assumed to be irreversibly broken. The lifetime of the chain was then taken to be the final time that the irreversibly dissociated bond had exceeded r_m. Trajectories of at least 15 times the average chain lifetime were propagated to allow for irreversible decay. These plots yielded the decay rates associated with no recrossings (k_{MD}) and with recrossings ($k_{MD,rec}$), respectively.

In order to obtain decay rates that could be compared to those predicted by statistical theories, the decay plots were considered to have an exponential form so that time-independent, first-order rates could be associated with the chain decay. However, as has been mentioned, even under microcanonical conditions

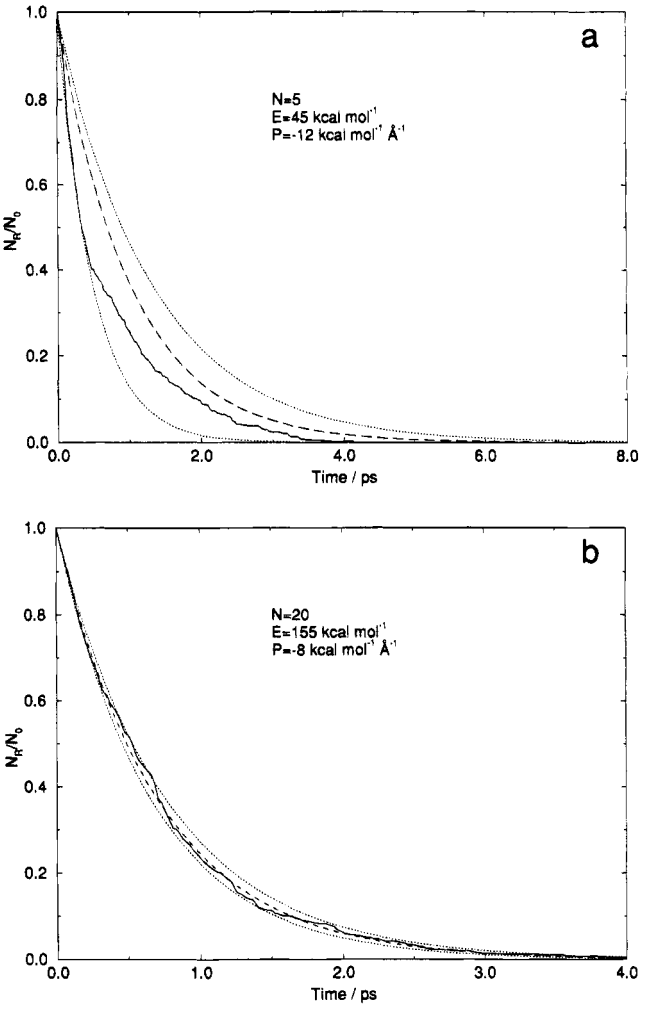

Figure 4. Decay curves (solid lines) of a 5-atom (panel a) and 20-atom (panel b) chain. The decay curve in panel b shows single-exponential behavior and thus has a smaller associated range (dotted lines) than the curve in panel a. The curve associated with the overall decay rate (dashed curve) lies within the decay range.

it is seldom that the decay plot can be accurately approximated by a single exponential. A range of MD decay rates was therefore associated with each decay curve by performing a least-squares fit of an exponential function to different regions of the decay plot. Thus, the decay curve was apportioned into 20 sections such that each section contained 5% of the dissociated trajectories. The decay data in each section were then fitted, using least-squares procedures, to the exponential function e^{-kt}.

The rate constant obtained from least-squares fitting to the complete (unapportioned) decay curve was obtained for the 3, 5, 10, and 20 atom chains. The bootstrap method[31,32] was used to determine the standard deviation of these decay rates. A total of 1000 samples of 500 trajectories were used to obtain the error estimates.

Apart from the fact that the range of MD decay rates can be used to compare to the statistical predictions, it can also be used to assess the degree of nonexponentiality of the decay. A large range indicates a highly nonexponential form of the decay curve while a small range indicates that the decay is essentially single exponential. Figure 4 shows MD decay plots obtained for 5- and 20-atom chains. Both curves are obtained assuming that the chain had decayed after the first crossing. Figure 4a was obtained at a energy of 45 kcal mol^{-1} and a pressure of -12 kcal mol^{-1} Å^{-1} while Figure 4b was obtained at an energy of 155 kcal mol^{-1} and a pressure of -8 kcal mol^{-1} Å^{-1}. The

curve in Figure 4b is closer to a single-exponential curve than that in Figure 4a,[35] and thus the associated range of MD decay rates—1.51 − 1.30 = 0.21 ps^{-1}—is smaller than the range calculated for the curve in Figure 4a—1.29 ps^{-1}. The fourth curve shown in these figures is the decay plot obtained from the least-squares fit to the complete decay curve. As expected, this curve lies within the range of MD decay rates.

In addition to determining the decay plots, the MD trajectories were used to calculate lifetime distributions and time-dependent rate constants. The lifetime distribution is obtained from the time of decay (*i.e.*, the time that the dissociating bond exceeds the critical bond length for the first time, corresponding to no recrossings, or the final time, corresponding to irreversible decay) of each trajectory in the ensemble. The time-dependent rate constant is related to the number of trajectories that dissociate at any instant (or within a small time interval) over the decay period. The methods used to calculate these quantities have been described previously.[22]

Multiple-Chain Systems. The investigation of the fragmentation of a single chain under stress was extended to the dissociation of arrays of chains (see Figure 2) under similar conditions. Since the main objective of this part of the investigation was to ascertain the effect of barrier recrossings, the investigation was limited to 5 and 10 atom chains. As will be discussed, an increase in tensile stress has the same qualitative effect on the decay rate as an increase in energy. For this reason, only the energy dependence of the decay rate is investigated. It will also be seen that, although recrossings affect the decay rate of the five-atom chain, these effects are small in comparison to those observed for the 10-atom chain. These two chain lengths were thus chosen to observe the effects of recrossings (induced by incorporating the chain into an array) on a chain where recrossings play a negligible role under single chain conditions and where recrossings play a significant role.

The chains comprising the array are independent except for the coupling via the shared end atoms. The Hamiltonian for this system is

$$H_{arr} = \sum_{j=1}^{N_{ch}} \{ \sum_{i=1}^{N-1} D_e(1 - e^{-\beta r_i - r_e})^2 + \sum_{i=1}^{N} {}^1/_2 m_i v_i^2 \} + Pr_c \quad (25)$$

where N_{ch} is the number of chains in the array. The position and velocity of the end atoms of each chain, which form the "walls" of the array, are the same for all chains. The walls have a mass of $N_{ch}m_i$. P is the pressure on the array. (The array "length" equals the length of the individual chains, r_c.)

The decay rate of the array that is predicted by statistical theory is

$$k_{arr} = (\tau_{arr})^{-1} \quad (26)$$

where τ_{arr} is the lifetime of the array as defined earlier. Since the fragments of the dissociating chains are no longer free to move apart (as they were in the single-chain systems) due to the presence of the walls, the calculation of the decay rate constant based on the separating fragment masses loses its relevance. The array dissociation rate constants were thus based on the reduced mass of the atoms that form the dissociating bond.

The kinematic coupling that exists between the chains in the array due to the sharing of the end atoms allows for fluctuations in chain energy. Thus, although each chain has microcanonical initial conditions, the energy in the chains will not be time independent. A decay rate constant based on microcanonical theories (*i.e.*, constant chain energy) will therefore only be applicable when the effects of fluctuations are negligible, and a decay rate based on thermal statistical theories is likely to overestimate the effects of energy fluctuations. Both types of rates were determined with the expectation that the thermal rate constant will be an upper limit for statistical systems (*e.g.*, when IVR is rapid). Two rate constants were thus determined: $k(T)_{arr}$ was obtained from the nucleation theory and $k(E)_{arr}$ from the corresponding anharmonic microcanonical theory.

The predicted decay rates were compared to the rates obtained from MD simulation. The initial coordinate selection was performed as in the case of the single chain with modifications required for the simulation of the array:

1. N_{ch} chains were chosen by the MC procedure before the array was propagated.

2. The end atoms of each chain had positions and velocities that were determined by the first MC selection procedure. These end atom coordinates were thus fixed for the remaining $N_{ch} - 1$ chains.

3. The center-of-mass motion of the two end atoms was calculated by assuming that they had a mass of $N_{ch}m_i$, where m_i is the atomic mass of bromine. The velocities of the middle atoms (nonend atoms) of each chain were then chosen with the restriction that the center-of-mass motion of these atoms was $1/N_{ch}$ of the sum of the center-of-mass motion of the end atoms. This gave a zero overall center-of-mass motion for the array.

4. The kinetic energy associated with the end atoms was calculated and included in the weighting procedure of the Markov chain (for the last $N_{ch} - 1$ coordinate selections) as

$$W_{trial} = 0, \quad V_N \geq E - E_{com} \quad (27)$$

where E_{com} is the kinetic energy of the end atoms determined in the first Monte Carlo selection step plus the minimum kinetic energy required by the central (nonend) atoms to achieve zero center-of-mass momentum of the chain. The MD simulation of the array was done by assuming a mass of $N_{ch}m_i$ for each end atom. Apart from conserving the zero linear momentum criterion throughout the simulation, this assumption gives the "walls" that enclose the array a mass that is a factor of N_{ch} larger than that of an atom in the chains. Ensembles of 500 trajectories were propagated for each chain length and energy.

The decay of arrays consisting of 3, 5, and 7 chains was investigated. Three decay plots were obtained for the arrays at each energy and chain length:

1. The decay associated with the first time that any bond (in any chain) exceeded the critical bond length. This corresponds to the reversible decay described for the single chain and gives a range of MD decay rates (and overall decay constant) k_{MD}.

2. The irreversible decay rate is associated with trajectories that do not recross the reaction barrier after array breakage. Thus, if chain i is the last chain to break before all chains have broken irreversibly (defined by the same criterion as before), the time of irreversible decay is the last time that bond j of chain i exceeds the transition state length where bond j is the bond that breaks irreversibly. This yields $k_{MD,irr}$.

3. The decay is also determined from the first time that all chains in the array simultaneously have at least one bond which is longer than the critical bond length. This gives $k_{MD,rev}$ and should not be confused with k_{MD} defined in the first point.

Results and Discussion

Single-Chain Results. A time-independent rate constant—which is predicted by RRKM theory—implies an exponential lifetime density and an exponential decay. A deviation

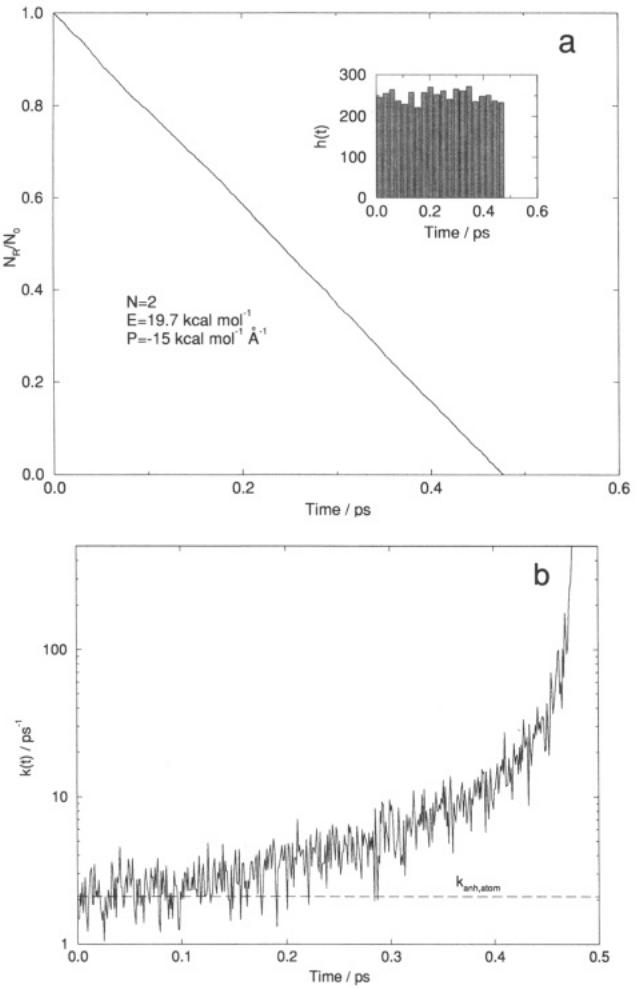

Figure 5. Decay rate (panel a), lifetime distribution (insert), and time-dependent rate constant (panel b) typical for a diatomic chain. The decay rate predicted by RRKM theory is shown as the dashed line in panel b. It is evident that the decay is nonstatistical.

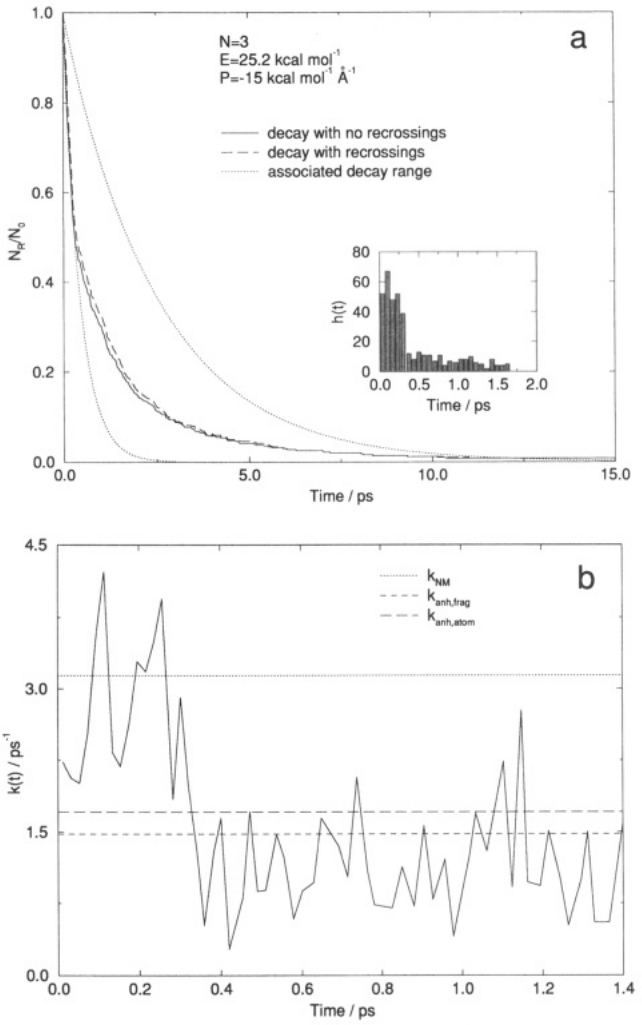

Figure 6. Same as Figure 5 but for a triatomic chain. The dotted curves in panel a show the decay range associated with the solid curve (*i.e.*, recrossings not taken into account).

from this behavior will indicate that the assumptions made by this theory are not applicable to our one-dimensional chain decay. Thus, although this is not a sufficient requirement to confirm the accuracy of RRKM predicted decay rates, the time independence of the rate constant and the exponential shape of the decay and lifetime distribution are necessary features of RRKM-type decay.

Figure 5 shows the lifetime distribution, decay plot, and time-dependent rate constant for the limiting case of a diatomic chain at an energy of 19.7 kcal mol^{-1} and a pressure of -15 kcal mol^{-1} Å^{-1}. The lifetime distribution gives the number of trajectories (y axis) that decays in a certain time interval (x axis). The decay plot shows the ratio of the number of reactant chains (trajectories which have not dissociated) to the number of chains in the ensemble as a function of time. The time-dependent rate constant is related to the number of trajectories that dissociate within a fine-grained time interval.[22] The shape of these curves is typical for the diatomic chain over all energies and pressures investigated. The lifetime distribution (see the insert of panel a) is a step function which falls to zero at the period of oscillation (0.48 ps) since the diatomic chain, which is given a random initial bond length, will dissociate when the bond length exceeds the critical length. As expected, there are no recrossings of the diatomic chain under stress. Dissociation which yields a step function lifetime distribution will exhibit linear decay as shown in Figure 5a. The time-dependent rate constant shown in Figure 5b is clearly not a constant of the motion. Comparison with the RRKM predicted rate constant—shown as the (time-independent) dashed line in Figure 5b—reveals that these rate constants are equal at $t = 0$ but that the time-dependent rate constant exceeds the RRKM prediction at longer times. The features associated with diatomic chain decay are thus in disagreement with RRKM predicted behavior. These results and conclusions agree with those of the diatomic chain with no external pressure reported previously.[22] They serve to remind us that the shortest chain (which can be studied analytically) does not decay statistically.

Figure 6 shows corresponding plots for the triatomic chain at an energy of 25.2 kcal mol^{-1} and a pressure of -15 kcal mol^{-1} Å^{-1} and is typical for triatomic chains at all energies and pressures. The plot of the lifetime distributions is not an RRKM-type exponential curve but shows a distinct separation of trajectories that have a short lifetime (direct trajectories) and those with a longer lifetime (complex trajectories).[36] The direct trajectories (whose decay characteristics are similar to those observed for the diatomic chain) are nonstatistical and have a step function lifetime distribution, while the complex trajectories show an approximately exponential lifetime distribution that is associated with statistical decay. This is a result of the slow internal vibrational relaxation (IVR) which is characteristic of triatomic chains.[22] The slow IVR is also evident in the decay curves shown in Figure 6a which illustrate the nonexponential behavior associated with this phenomenon. Decay curves of this type—*i.e.*, a superposition of a linear decay (direct trajec-

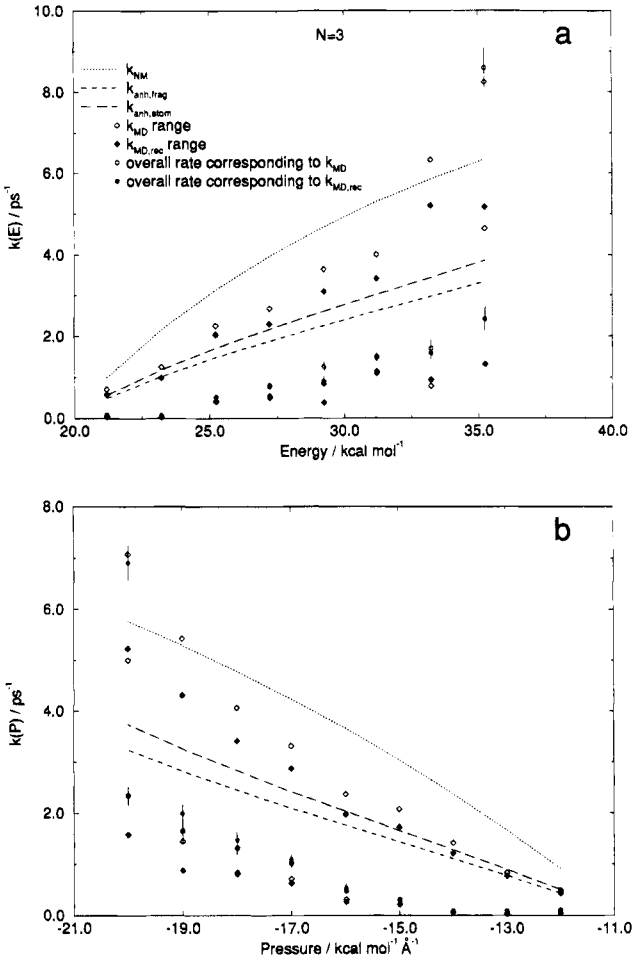

Figure 7. Energy (panel a) and pressure (panel b) dependence of the predicted and MD determined microcanonical rate constants for the triatomic chain. Data in panel a were obtained at a pressure of -15 kcal mol^{-1} Å^{-1} (E_0 at this pressure is 19.74 kcal mol^{-1}) and that in panel b at an energy of 25.0 kcal mol^{-1}. Error bars were obtained using the bootstrap method. k_{MD} and $k_{MD,rec}$ are the ranges spanned by the vertically aligned filled and unfilled diamonds, respectively.

tories) and an exponential decay (complex trajectories)—will be characterized by a large range of MD decay rates as indicated by the (dotted) exponential curves in the figure. (The curves that are illustrated were obtained from fitting to the decay plot where recrossings were not taken into account.) It is also evident that recrossing does not affect the rate of decay of the triatomic chain at this energy and pressure. From Figure 6b it can be seen that the time-dependent rate constant lies well above the time-independent rate ($k_{anh,frag}$ and $k_{anh,atom}$) at shorter times and below it at longer times. Once again, this shows behavior that is typical for a system that has slow internal energy redistribution.

In Figure 7 we compare the rate constants obtained from MD simulation of the triatomic chain to those predicted by the different forms of the RRKM theory. The harmonic RRKM theory, which is the simplest and most widely used form of the theory, yields decay rates that are larger than the anharmonic decay rates and the MD determined rates (except at high energies and negative pressures). The omission of anharmonic effects clearly leads to an overestimation of the rate constant. The dissociation rates $k_{anh,atom}$ and $k_{anh,frag}$ are fairly similar since the difference between the reduced mass of the dissociating fragments and that of the dissociating atoms is not large enough to lead to a significant change in the decay rate. This, together with the fact that a large range of MD decay rates is obtained for k_{MD} due to the nonexponential decay curve, leads to good agreement between both predicted anharmonic RRKM results and the range of decay rates obtained from MD simulation. The negligible effect that recrossings have on the decay rate (as seen in Figure 6a) is illustrated by the fact that the ranges of MD decay rates spanned by the filled diamonds in Figure 7 (which shows $k_{MD,rec}$) are equal to the range of k_{MD} (unfilled diamonds). Thus, even though the decay rates predicted by the anharmonic RRKM theories are well within the ranges of MD decay results, the triatomic chain does not show RRKM-type decay, lifetime distribution, or a time-independent rate constant.

Figure 7 also shows a general increase in the range of k_{MD} at higher energies and more negative pressures. This is due to the fact that as one increases the energy (above E_0) so one increases the probability of inserting sufficient energy in a particular bond (or region of the chain for $N > 3$) which may lead to dissociation within one (or a few) periods. This affects the fast rate constant, *i.e.*, the upper value of the k_{MD} range, more than the slow rate constant, which is dependent on the rate of IVR, so that the range of k_{MD} will be extended at higher energies. At very high energies, where the energy is similar to the sum of the bond dissociation energies, the dissociation rates will be similar in magnitude to the bond frequencies (assuming no effects of the surrounding atoms). This type of decay, *i.e.*, where the initial energy in a bond is greater than the barrier height so that fission occurs on a faster time scale than IVR, will be similar to that of a diatomic chain. As seen in Figure 5b, this will lead to k_{MD} rates that are well above the anharmonic RRKM rates. An example of this behavior is seen in Figure 7a at an energy of 35.2 kcal mol^{-1} (which is almost equal to $2E_0 = 2 \times 19.7 = 39.4$ kcal mol^{-1}) and in Figure 7b at a pressure of -20 kcal mol^{-1} Å^{-1} (where the energy is 25.0 kcal mol^{-1} and $2E_0 = 2 \times 14.4 = 28.8$ kcal mol^{-1}). The improved agreement between the MD decays and the harmonic RRKM rates at these high energies and pressures is fortuitous. Finally, it is only at these high energies and pressures that recrossings lead to a significant change in the decay rate. This is due to the fact that at high energies the motion of the chain atoms is essentially uncorrelated so that the dissociating atoms are more likely to be "knocked back" by the third atom than at low energies where the dissociation occurs when the dissociating fragments are separating in phase (*i.e.*, according to the chain normal mode eigenvectors).

The exponential form of the decay and lifetime distribution predicted by RRKM theory becomes apparent at longer chain lengths. An example of this is shown in Figure 8 for the 10-atom chain at an energy of 110.0 kcal mol^{-1} and a pressure of -8 kcal mol^{-1} Å^{-1}. Figure 8a shows that both the decay plot and the lifetime distribution (see inset) approach single-exponential behavior. The decay obtained from the first dissociating bond crossing (which yields k_{MD}) and that determined from the final crossing (which yields $k_{MD,rec}$) are plotted. It is clear that the recrossings affect the MD determined rate constant of the 10-atom chain at this energy and pressure. Figure 8b shows that the rate constant (obtained when neglecting recrossings) is essentially time independent for this chain under these conditions. It is also apparent that $k_{anh,atom}$ is a better prediction than $k_{anh,frag}$ or k_{NM}. The reasons for this are the same as those discussed in the case of the triatomic chain and will be discussed in more detail below.

Figure 9 shows the RRKM predicted and MD determined rate constants for the 5-, 10-, and 20-atom chains as a function of energy. The behavior of the rate constant with increasing negative pressure is the same as that with increasing energy (*e.g.*, as observed in Figure 7), and thus these plots are not shown. It is instructive to note that the information shown in

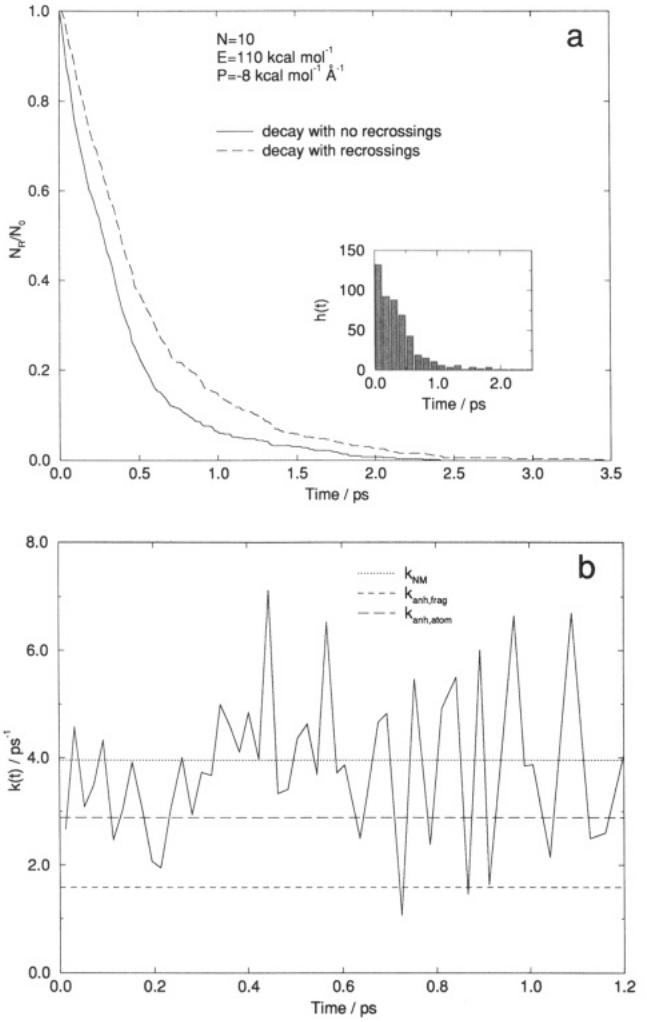

Figure 8. Same as for Figure 5 but for a 10-atom chain. The data shown are characteristic of statistical decay.

Figure 8a,b is also shown in Figure 9b at an energy of 110.0 kcal mol^{-1}. The $k_{MD,rec}$ range (shown by the filled diamonds in Figure 9b) is clearly different from the k_{MD} range shown by the unfilled diamonds. Both ranges of MD decay rates are fairly small, indicating the good exponential shape of the decay curves. $k_{anh,atom}$ clearly gives a better prediction of k_{MD} at this energy than $k_{anh,frag}$ or k_{NM}. This is in agreement with the data seen in Figure 8.

The discussion concerning the triatomic chain decay rates (based on Figure 7) can be extended to the curves shown in Figure 9. It is evident that there is an increase in the rate constant and the range of decay rates determined from MD with increasing energy. Except for very high energies—where the probability of dissociation occurring on a time scale equivalent to that of a bond vibrational period increases dramatically—the rate constant predicted by harmonic RRKM theory serves as an upper bound to the rate obtained from MD simulation. At low energies $k_{anh,frag}$ and $k_{anh,atom}$ predict values within the k_{MD} and $k_{MD,rec}$ ranges. At these lower energies the chain atoms behave in a correlated manner (*i.e.*, this is near the normal mode limit), and thus there are no significant effects due to recrossing. As the energy is increased (or the negative pressure is increased at constant energy), the correlation between the atomic motions diminishes. This has two effects: First, the k_{MD} range is better predicted by $k_{anh,atom}$ (see Figure 9) since the local mode—rather than the normal mode—picture of atomic vibrations is relevant. Second, recrossing plays a more important role since the uncorrelated motion of the atoms leads to the dissociating bond being pushed back to the reactant region of phase space. The $k_{MD,rec}$ and k_{MD} ranges will thus diverge as shown in Figure 9. Clearly, an increase in chain length, which means that in general there will be more atoms surrounding the dissociating bond, will lead to larger recrossing effects. Hence, for longer chains such as the 20-atom chain, the effects of recrossing may be

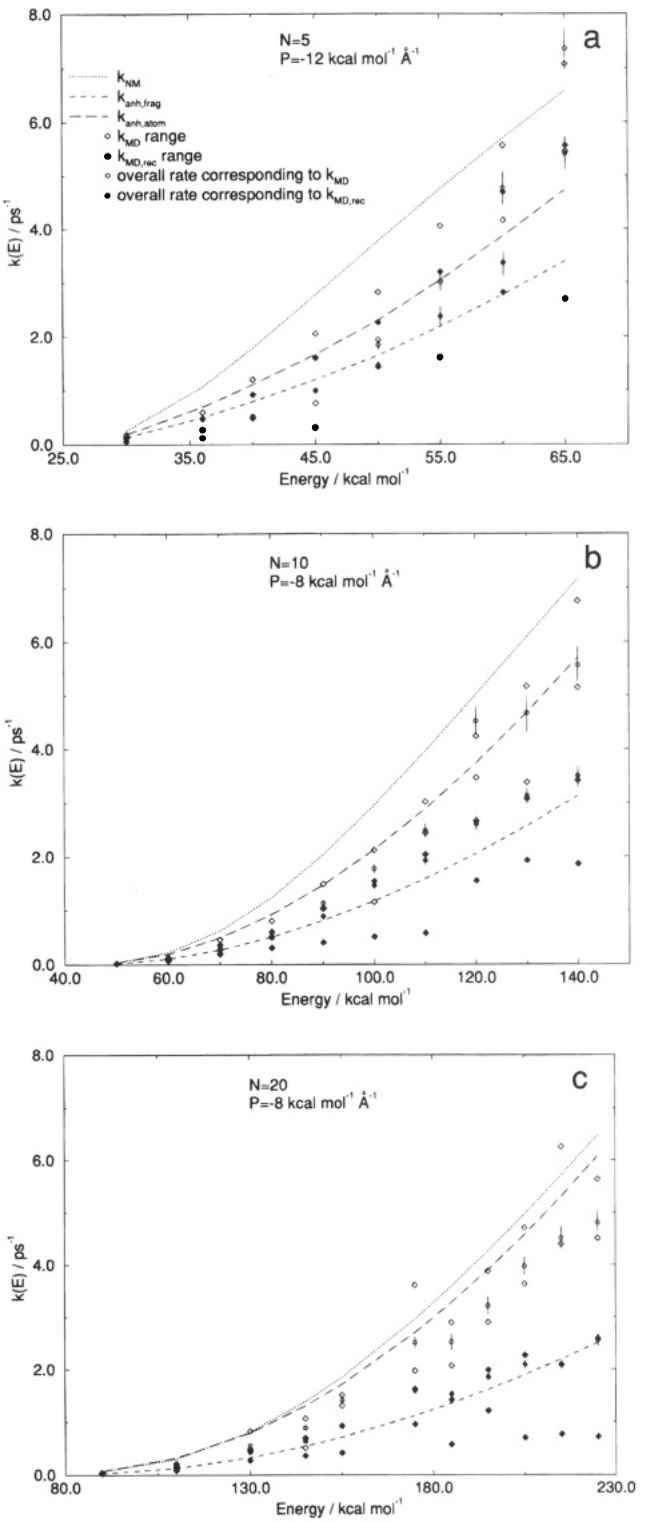

Figure 9. Energy dependence of the predicted and MD determined rate constants of the 5- (panel a), 10- (panel b) and 20-atom (panel c) chain systems under microcanonical conditions. The legend in panel a applies to all panels. k_{MD} and $k_{MD,rec}$ are the ranges spanned by the vertically aligned filled and unfilled diamonds, respectively. It is evident that the rate constants predicted by the statistical theories which incorporate anharmonic effects are in better agreement with the MD results than are the RRKM predicted rate constants.

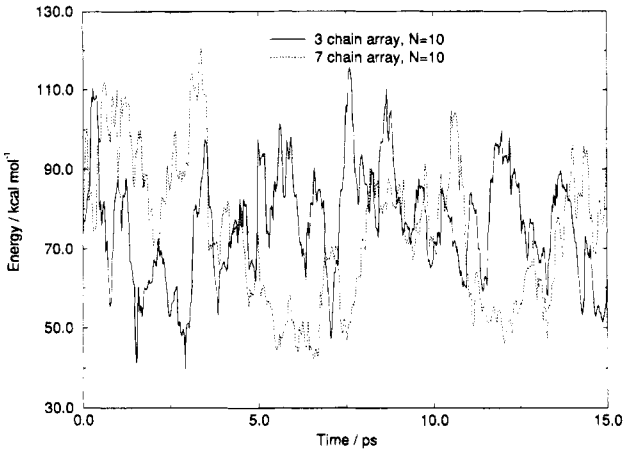

Figure 10. Chain energy as a function of time. The solid curve shows typical energy fluctuations in a chain of an array comprising three chains, and the dotted curve is obtained from a chain of the seven-chain array. Each chain (in both array sizes) consists of 10 atoms and has an initial energy of 76.0 kcal mol^{-1} and a pressure of −8 kcal mol^{-1} $Å^{-1}$.

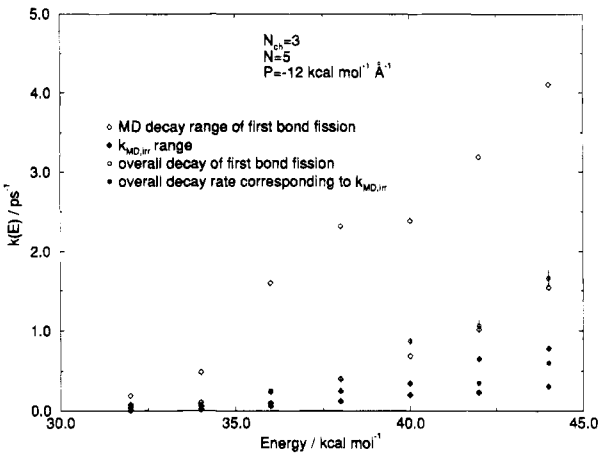

Figure 11. MD determined array decay rates for the three-chain array with five atoms in each chain. The effect of recrossings increases with energy.

large enough to lower the decay rate to the extent that $k_{anh,frag}$ is a better prediction than $k_{anh,atom}$. Increasing the negative pressure (at constant energy) has the same effect as increasing the energy (at constant pressure) since the barrier height for decay, E_0, is lowered at more negative pressures.

Multiple-Chain Results. The fluctuations in the energy of the chains that comprise the arrays are represented in Figure 10. The solid curve is the time-dependent energy of a single chain of the three-chain array (10 atoms in each chain), and the dotted curve is the energy of one of the chains that forms part of the seven-chain array (10 atoms in each chain). The features observed are typical of the other chain lengths and arrays that have been studied. The energies are plotted over the first 15 ps, where the initial chain energies are 76.0 kcal mol^{-1} (the pressure is −8 kcal mol^{-1} $Å^{-1}$). It is evident that there are significant fluctuations in the chain energies. The effect of these fluctuations is twofold: The decay rates obtained from microcanonical theory may underestimate the rate of dissociation, and the large flow of energy into a chain may induce nonstatistical breakages of that chain. (It will be remembered that this effect was observed in the single-chain systems at high energies.) Thus, at moderately high energies where fluctuations in energy are expected be significant, $k(T)_{arr}$ may be a better prediction than $k(E)_{arr}$.

Figure 10 also shows that there is not a significant increase in the amplitude of the fluctuations when increasing the number of chains in the array. Thus, the coupling between the chains is sufficiently weak so that an increase in the total energy of the system (obtained by adding more chains to the array) does not lead to increased fluctuation amplitudes. An increase in the number of chains, N_{ch}, in the array leads to a proportionate increase in the mass of the walls and thus a decrease by a factor of $1/N_{ch}$ of the kinematic coupling between each chain. Thus, the overall leakage of energy from one chain to all the others in the array (interchain IVR) can be expected to scale as $(N_{ch} - 1)/N_{ch}$, and thus the fluctuation amplitudes of the chain energy should become independent of N_{ch} for a sufficiently large array. The relative decay rate of arrays with different number of chains will therefore be govered by the difference in "tensile strength" of these arrays (and not by the change in total energy).

The constraints that the walls of the array place on the motion of the separating chain fragments are expected to lead to a large number of recrossings. This effect is illustrated for a three-chain array with five atoms in each chain in Figure 11. The symbols used in this figure are the same as those used in Figure 9a in order to facilitate direct comparison between these figures. The pressure was −12 kcal mol^{-1} $Å^{-1}$ in both cases. The unfilled diamonds show the range of MD decay rates associated with the first bond fission (*i.e.*, any bond in the array) while the filled diamonds give the range of MD decay rates associated with the irreversible decay rate (determined under the same criterion pertaining to the single chains). It is clear that the effect of recrossing has increased dramatically due to the inclusion of many chains in the array. The effect of recrossings will lead to an overestimation of the decay rate predicted by statistical theories.

Figure 12 shows the decay rates of the 3, 5, and 7 chain arrays as a function of energy. There were 10 atoms in each chain. The results obtained from the arrays of five-atom chains have similar trends to those shown. The total pressure on the array, −8 kcal mol^{-1} $Å^{-1}$, is the same as that used in the corresponding single-chain investigations. The energies shown on the x axis are the initial energies of the individual chains in the array. The unfilled squares give the range of MD decay rates determined from the first time that all chains in the array are simultaneously broken (the triangles and error bars are the corresponding overall decay rates), and the filled diamonds give the range associated with the irreversible MD decay rates (the filled circles and error bars are the related overall decay rates). The same symbols that were used in the single-chain comparison have been used in order to facilitate easy comparison with Figure 9b.

It is clear from Figure 12 that $k_{MD,rev}$ (unfilled squares) and k_{MD} have similar ranges. $k_{MD,rev}$ should not be confused with the "reversible" decay rate that pertains to individual chains and that was discussed with reference to Figure 11. The statistical predictions assume no recrossings after the *individual chains* have broken, and as has been discussed, this is a poor assumption when array dissociation is considered. However, it is apparent from Figure 12 that once all chains have at least one bond extended past the critical configuration at the same time, there is a negligible effect of recrossing. This is expected since once all chains are simultaneously broken, it is improbable that excursions of individual chains back into the reactant region of phase space will prevent the separation of the two massive array fragments that are under the influence of the pressure.

A comparison of the decay rates as a function of number chains in the array (using Figures 12 and 9b) shows that the decay rate decreases with increasing number of chains in the array. This is valid even though the total energy in the array increases in proportion to the number of chains (each chain has

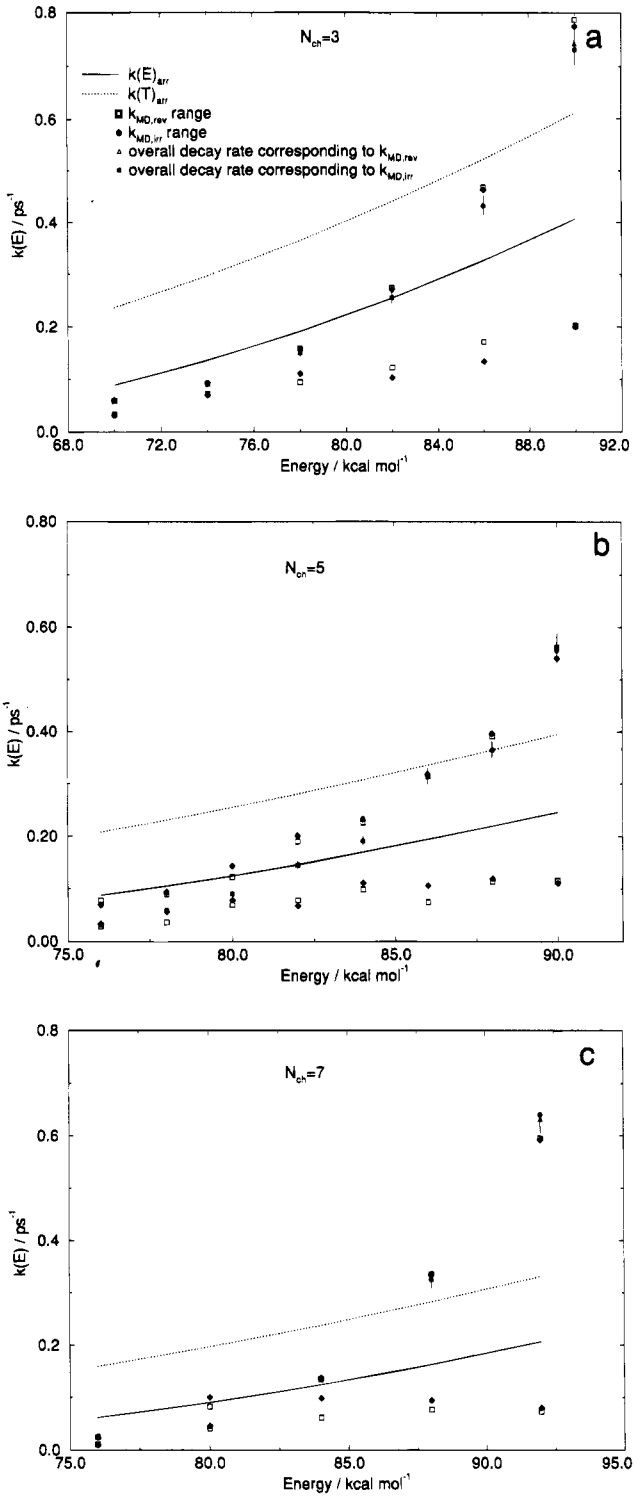

Figure 12. Predicted and MD determined array decay constants as a function of energy. In all cases the chains consist of 10 atoms (3, 5, and 7 chain arrays are shown in panels a, b, and c, respectively), and the pressure was -8 kcal mol^{-1} Å^{-1}. The legend in panel a applies to all panels. $k_{MD,rev}$ and $k_{MD,irr}$ are the ranges spanned by the unfilled squares and unfilled diamonds, respectively.

an initial energy shown on the x axis). The reason for this has been alluded to above: The fluctuations in the chain energy are essentially independent of the number of chains in the array, and thus the fission of individual chains is independent of the increase in the array energy obtained by the addition of chains. Therefore, the most important factor governing array dissociation rate is not the total energy of the array, but rather the energy of the individual chains and the number of chains in the array that increase the tensile strength. An increase in the number of chains will decrease the pressure that is applied to the individual chains (given that the total pressure on the array is constant), which will lead to a decrease in the decay rate.

It is also evident (from Figure 12), that, in general, the microcanonical decay rate affords a better prediction than the thermal decay rate at low energies, a MD decay rate that lies between these two predictions is found at intermediate energies, and at high energies the MD decay ranges exceed even the thermal decay rate predictions. This is explained as follows: At low energies the fluctuations are small, and thus the microcanonical theory is applicable and hence gives the best predictions. As the energy and fluctuations increase, the decay rate exceeds that predicted by the microcanonical theory and the thermal decay predictions give an upper bound. At high energies the fluctuations are large so that nonstatistical effects are significant: Large fluctuations in chain energy will lead to an increased probability of the end bonds having high energy (since the chains are linked via the end atoms). This leads to decay rates in excess of the RRKM prediction as discussed for the single chains (Figure 5b and 7) and hence to an increase in the magnitude of the range of MD decay rates (as in the case of the single chain), and the thermal decay prediction is no longer an upper bound.

Conclusion

This investigation has employed a simple one-dimensional chain model to compare the rate constants obtained from MD simulation to those predicted by microcanonical statistical (RRKM) theory. Nonstatistical phenomena (*e.g.*, barrier recrossing and slow IVR) observed under constant-energy conditions also appear under the corresponding thermal conditions, and thus the applicability of the RRKM theory examined in this work is directly related to the applicability of the corresponding canonical nucleation theory under thermal conditions.

The diatomic and triatomic chains yielded decay curves and lifetime distributions that were nonexponential, while the decay rate constants associated with these chains were time dependent. This led to the conclusion that these chains could not be described in terms of RRKM theory even though in the case of the triatomic chain the RRKM prediction fell between the two limits of the nonexponential decay.

An increase in chain length led to decay behavior that is predicted by RRKM theory, but the fit to a single-exponential shape deteriorated with increasing energy and negative pressure due to rapid bond breakage and barrier recrossings. In the regions where these nonstatistical effects were not too large, the harmonic RRKM theory predictions gave an upper bound to the MD determined decay rate. The effect of recrossings on the decay rate is more important for longer chains at higher energies and more negative pressures where they can lead to a significant lowering of the rate of decay, thereby bringing it closer to the anharmonic RRKM rate constant that was determined using the fragment masses.

The investigation of the array decay rates showed that it is necessary to take account of the fluctuation in energies of the chains comprising the array even when the coupling between the chains is extremely weak. The presence of the fluctuations limits the applicability of microcanonical statistical theory (where individual chains are assumed to have constant energy) to low energies where the fluctuations are small. Predictions from a thermal statistical theory gave improved predictions at higher energies, but even at moderately high energies the fluctuations led to nonstatistical effects that rendered both types of statistical predictions inapplicable.

Since it has been observed that nonstatistical effects do not have a significant influence on the decay rate and mechanism at lower energies and pressures, we suggest that a microscopic statistical nucleation theory may be suitable under conditions that yield experimentally observable nucleation times. The results obtained from the array simulations show that barrier recrossing may pose a severe limitation when the theory is applied to a realistic three-dimensional system. However, even in this case it is evident that the significance of the nonstatistical effect reduces dramatically with decreasing energy (and hence also with decreasing temperature) so that it may not pose as large a problem under conditions relevant to experimentally observable nucleation times.

Acknowledgment. K.B. is grateful for the financial support obtained from the Swedish Natural Science Research Council and the Foundation for Research Development, South Africa. H.W.S. is grateful for financial support from the Australian Research Council through the award of an ARC Research Fellowship.

References and Notes

(1) Robinson, P. J.; Holbrook, K. A. *Unimolecular Reactions*; Wiley-Interscience: New York, 1972.
(2) Forst, W. *Theory of Unimolecular Reactions*; Academic Press: New York, 1973.
(3) Slater, N. B. *Theory of Unimolecular Reactions*; Cornell University Press: Ithaca, NY, 1959.
(4) Crim, F. F. *Annu. Rev. Phys. Chem.* **1984**, *35*, 657.
(5) Stephenson, J. C.; Bialkowski, S. E.; King, D. S.; Thiele, E.; Stone, J.; Goodman, M. F. *J. Chem. Phys.* **1981**, *74*, 3905.
(6) Truhlar, D. G.; Hase, W. L.; Hynes, J. T. *J. Phys. Chem.* **1983**, *87*, 2664.
(7) Reddy, K. V.; Berry, M. J. *Chem. Phys. Lett.* **1979**, *66*, 223.
(8) Wolters, F. C.; Rabinovitch, B. S.; Ko, A.-N. *Chem. Phys.* **1980**, *49*, 65.
(9) Schatz, G. C.; Buch, V.; Ratner, M. A.; Gerber, R. B. *J. Chem. Phys.* **1983**, *79*, 1808.
(10) Reinhardt, W. P.; Duneczky, C. *J. Chem. Soc., Faraday Trans. 2* **1988**, *84*, 1511.
(11) Schranz, H. W.; Raff, L. M.; Thompson, D. L. *J. Chem. Phys.* **1991**, *94*, 69.
(12) Schranz, H. W.; Raff, L. M.; Thompson, D. L. *J. Chem. Phys.* **1991**, *95*, 106.
(13) Sewell, T. D.; Schranz, H. W.; Thompson, D. L.; Raff, L. M. *J. Chem. Phys.* **1991**, *95*, 8089.
(14) Schranz, H. W.; Raff, L. M.; Thompson, D. L. *Chem. Phys. Lett.* **1991**, *182*, 455.
(15) (a) Chapman, S.; Uzer, T. In *Advances in Classical Trajectory Methods*; Hase, W. L., Ed.; JAI Press: New York, 1992. (b) Davis, M. J.; Skodje, R. T. *Ibid.* (c) Duneczky, C.; Reinhardt, W. P. *Ibid.* (d) Ezra, G. S. *Ibid.* (e) Hutchinson, J. S. *Ibid.* (f) Rice, S. A.; Gaspard, P.; Nakamura, K. *Ibid.*
(16) (a) Clarke, D. L.; Collins, M. A. *J. Chem. Phys.* **1990**, *93*, 7894. (b) Hutchinson, J. S.; Reinhardt, W. P.; Hynes, J. T. *Ibid.* **1983**, *79*, 4247. (c) Talanina, I. B.; Collins, M. A. *Ibid.* **1993**, *98*, 1817. (d) Collins, M. A. *Physica D* **1993**, *63*, 138.
(17) Hutchinson, J. S.; Wyatt, R. E. *Phys. Rev. A* **1981**, *23*, 1567.
(18) Hutchinson, J. S.; Hynes, J. T.; Reinhardt, W. P. *Chem. Phys. Lett.* **1984**, *108*, 353.
(19) Fermi, E.; Pasta, J.; Ulam, S. Los Alamos Scientific Laboratory Report LA-1940, 1955.
(20) Rice, S. A. *Adv. Chem. Phys.* **1981**, *97*, 117.
(21) Rice, S. A. In *Advances in Laser chemistry*; Zewail, A., Ed.; Springer-Verlag: Berlin, 1979.
(22) Schranz, H. W.; Nordholm, S.; Freasier, B. C. *Chem. Phys.* **1986**, *108*, 69.
(23) Schranz, H. W.; Nordholm, S.; Freasier, B. C. *Chem. Phys.* **1986**, *108*, 93.
(24) Schranz, H. W.; Nordholm, S.; Freasier, B. C. *Chem. Phys.* **1986**, *108*, 105.
(25) Abraham, F. F. *Homogeneous Nucleation Theory: The Presaturation Theory of Vapour Condensation*; Academic Press: New York, 1974.
(26) Kashchiev, D.; Firoozabadi, A. *J. Chem. Phys.* **1993**, *98*, 4690.
(27) Bolton, K.; Nordholm, S. *Chem. Phys.* **1994**, *182*, 263.
(28) Schranz, H. W.; Raff, L. M.; Thompson, D. L. *Chem. Phys. Lett.* **1990**, *171*, 68.
(29) (a) Dove, J. E.; Hippler, H.; Plach, J.; Troe, J. *J. Chem. Phys.* **1984**, *81*, 1209. (b) Brouwer, L.; Hippler.; Lindemann, L.; Troe, J. *J. Phys. Chem.* **1985**, *89*, 4608.
(30) Hammersley, J. M.; Handscomb, D. C. *Monte Carlo Methods*; Methuen: London, 1967.
(31) Efron, B. *SIAM Rev.* **1979**, *21*, 460.
(32) Diaconis, P.; Efron, B. *Sci. Am.* **1983**, *248*, 96.
(33) Since we do not consider the effects applying a compression to the chain, the terms stress or pressure refer to a tensile stress or negative pressure.
(34) The harmonic approximation was not used in the present work. The more accurate numerical solution of eq 5 was used instead.
(35) The curve in Figure 4b is better represented by a single-exponential decay than that in Figure 4a due to the difference in the chain lengths and because the energy per bond, $E/(N-1)$, is lower in the 20-atom chain (8.16 kcal mol^{-1}) than in the 5-atom chain (11.25 kcal mol^{-1}).
(36) Only the first 1−2 ps is shown in the figures of the lifetime distribution and time-dependent decay rate since it is within this time domain that the nonstatistical behavior is observed.

JP942025O